

Article

# Adaptive Backstepping Sliding Mode Control Based RBFNN for a Hydraulic Manipulator Including Actuator Dynamics

Duc-Thien Tran , Hoai-Vu-Anh Truong and Kyoung Kwan Ahn \* 

School of Mechanical Engineering, University of Ulsan Daehakro 93, Nam-gu, Ulsan 680-764, Korea; thientd@hcmute.edu.vn (D.-T.T.); truonganh241292@gmail.com (H.-V.-A.T.)

\* Correspondence: kkahn@ulsan.ac.kr; Tel.: +82-52-259-2282

Received: 4 February 2019; Accepted: 16 March 2019; Published: 26 March 2019



**Abstract:** In this paper, an adaptive robust control is investigated in order to deal with the unmatched and matched uncertainties in the manipulator dynamics and the actuator dynamics, respectively. Because these uncertainties usually include smooth and unsmooth functions, two adaptive mechanisms were investigated. First, an adaptive mechanism based on radial basis function neural network (RBFNN) was used to estimate the smooth functions. Based on the Taylor series expansion, adaptive laws derive for not only the weighting vector of the RBFNN, but also for the means and standard derivatives of the RBFs. The second one was the adaptive robust laws, which is designed to estimate the boundary of the unsmooth function. The robust gains will increase when the sliding variable leave the predefined region. Conversely, they will significantly decrease when the variable approaches the region. So, when these adaptive mechanisms are derived with the backstepping technique and sliding mode control, the proposed controller will compensate the uncertainties to improve the accuracy. In order to prove stability and robustness of the controlled system, the Lyapunov approach, based on backstepping technique, was used. Some simulation and experimental results of the proposed methodology in the electrohydraulic manipulator were presented and compared to other control to show the effectiveness of the proposed control.

**Keywords:** hydraulic actuator; manipulator; radial basis function neural network; backstepping technique; Taylor series expansion; Lyapunov approach

## 1. Introduction

Due to advantages such as high load efficiency, small size-to-power ratio, and fast response, hydraulic actuators have been widely investigated in construction [1,2], aerospace [3], motion simulator [4], as well as robotic area [5–7]. Boston Dynamics' hydraulic robots such as BigDog [5], Atlas [6], and SARCOS's robot exoskeletons [7] are some examples of advanced hydraulic robot system. One of the crucial challenges in control of the hydraulic manipulator is undesired behavior due to extremely nonlinear behaviors of the system and actuator dynamics, uncertainties of the system, and external disturbance.

In previous works [8,9], the actuator dynamics were usually excluded from the manipulator dynamics to simplify the control procedure. However, the uncertainties in actuator dynamics affects the control performance, as well as the stability of the whole system [10]. Consequently, the actuator dynamics have been considered in robotic control design in recent researches [10–18]. The system dynamics arises both unmatched and matched uncertainties in manipulator dynamics and actuator dynamics, respectively. Many studies have been provided to deal with these problems, which can be divided into two categories. Firstly, some advanced controllers have been investigated on system

dynamics which were expressed by taking derivative of the acceleration variable of the manipulator to including the actuator dynamics [10–13]. Their results proved the effectiveness of this approach. However, they meet the observable problems due to the noise measurement. On the other hand, some advanced controllers have been employed on the system dynamics, which includes the manipulator dynamics and actuator dynamics, independently [14–17]. So, they take advantages of the sensors which had already been equipped in the system. Additionally, these controllers have been developed based on the backstepping technique because it is well-known as a good technique for handling the matched and unmatched uncertainties [19]. The main property of backstepping design, is that it stabilizes the system states through a step-by-step recursive process [20]. However, classical backstepping design mainly supposes that the uncertainties and the disturbance are constant or slowly altering. To enhance the compensation capability of the backstepping control, some adaptive laws [21] have been used to cope with the uncertainties. But, the derivatives of the model uncertainty and the disturbance cannot reach to zero, the backstepping with adaptive laws is no longer relevant.

The sliding mode control (SMC) has been extensively used to control uncertain nonlinear systems with high dynamic uncertainties because of its robustness [22]. The fundamental idea of the SMC is to use a discontinuous control term for driving the controlled system's error state variables toward zero. Chattering effect may be activated in cases of large control gains used [23]. So, the adaptive mechanisms [24–28] have been provided to eliminate this effect and to improve the ability of the SMC, which is named an adaptive SMC (ASMC). However, the SMC is not good at dealing with the unmatched uncertainties in the nonlinear system. Considering the characteristics of ASMC and backstepping, it is possible to combine these methods together for reserving their advantages and reducing their limitation at the same time. In previous studies [14,15,17], the adaptive backstepping sliding mode control was applied to a manipulator including electric actuator dynamics for position control problem. The adaptive mechanism were developed based on linear regressor method [14,17], and least square-support vector machine [15]. Although their results proved that these controllers dealt well with the uncertainties and disturbances. Their structure and initial values are usually selected by designer's experiences, so it is challenging to employ them in practice.

Based on the works mentioned above, this paper presents an adaptive backstepping sliding mode control for position tracking control of a hydraulic manipulator including actuator dynamics. Because the actuator dynamics are considered in the control design, the system will include both the unmatched uncertainties in the manipulator dynamics and matched uncertainties in the actuator dynamics. Furthermore, the uncertainties usually contain both the unsmooth and smooth functions. Then, this paper will employ two adaptive mechanisms based on sliding mode control and backstepping technique. The main contributions of the paper are presented as follows:

- Since the adaptive approximators are developed based on the neural network and the Taylor series expansion, they can adapt not only the weighting vector, but also the mean and standard derivative of the gaussian function in the neural network to estimate the smooth functions effectively.
- The adaptive switching gain laws are provided to handle the unsmooth function without the predefined boundary of uncertainties. When it works together with the adaptive approximators, these adaptive mechanisms will help to improve the accuracy.
- The backstepping technique and Lyapunov approach theoretically prove the stability of the whole system with the existence of the matched and unmatched uncertainties.
- Finally, some simulations and experiments are carried out and compared with PID and backstepping sliding mode control to verify the efficiencies of proposed control.

The paper is organized as follows: Section 2 presents an electro-hydraulic manipulator dynamic, and it consists of a manipulator dynamic and an electro-hydraulic dynamic. The control design and the proof of stability and robustness are depicted in Section 3. Some simulation results, and some

discussions are shown in Section 4. Some conclusions and future works are provided in Section 5. Additionally, the appendixes present the definitions of some matrices and vectors.

## 2. Robot Manipulator Dynamics

### 2.1. Manipulator Dynamic without Actuators

The electro-hydraulic manipulator which is depicted in Figure 1 is a 3-DOF robot manipulator driven by two hydraulic rotaries in the link  $i^{th}$  ( $i = 1, 2$ ) and one cylinder in the last link.

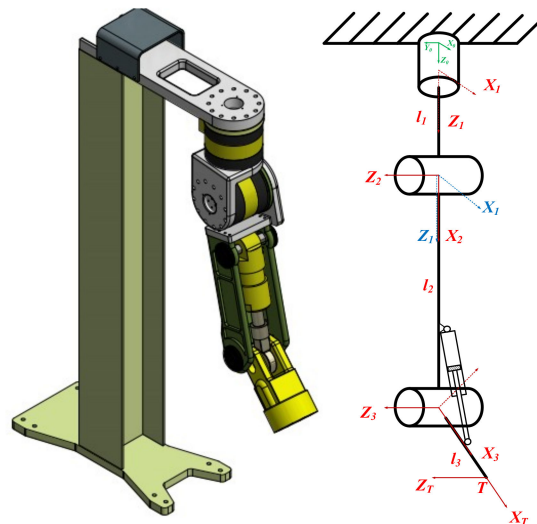


Figure 1. The structure of the 3-DOF manipulator.

Firstly, the manipulator dynamics in the joint coordinate are expressed by:

$$M(\theta)\ddot{\theta} + C(\theta, \dot{\theta})\dot{\theta} + G(\theta) + d(t) = \tau \tag{1}$$

where  $\theta, \dot{\theta}, \ddot{\theta} \in R^3$  are position, angular velocity and angular acceleration vectors of each joint, respectively,  $M(\theta) \in R^{3 \times 3}$  is the symmetric and positive definite matrix of inertia,  $C(\theta, \dot{\theta}) \in R^{3 \times 3}$  denotes the Coriolis and Centrifugal term matrix,  $G(\theta) \in R^3$  is the gravity term,  $\tau$  is torque acting on joints,  $\dot{M}(\theta) - 2C(\theta, \dot{\theta})$  is a skew-symmetric matrix [29], that is given as  $\theta^T (\dot{M}(\theta) - 2C(\theta, \dot{\theta}))\theta = 0$ , and  $d(t)$  stands for the disturbance induced in the hydraulic actuator and external factor while operating.

In fact, the robot dynamic parameters are not well known. Its dynamic is affected by the mass distribution, oscillation in the process of operation. Let's define  $M = M_0 + \Delta M$ ,  $C = C_0 + \Delta C$ ,  $G = G_0 + \Delta G$  where  $(\cdot)$  represents for estimated parameters which are clearly presented in Appendix A and  $\Delta(\cdot)$  acts as uncertainties of the model. Suppose that all  $\Delta(\cdot)$  are bounded, i.e.,  $\|\Delta\| \cdot \|\cdot\|_\infty \leq \xi(\cdot)$ , then the dynamic equation of the manipulator in (1) can be rewritten as:

$$M_0(\theta)\ddot{\theta} + C_0(\theta, \dot{\theta})\dot{\theta} + G_0(\theta) + \Delta U + d(t) = \tau \tag{2}$$

where  $\Delta U = \Delta M(\theta)\ddot{\theta} + \Delta C(\theta, \dot{\theta})\dot{\theta} + \Delta G(\theta)$  denotes the uncertainties of the system.

### 2.2. Electro-Hydraulic Dynamics

Let  $x_a = [x_{1a} \ x_{2a} \ x_{3a}]^T = [\theta_{1a} \ \theta_{2a} \ d_3]^T \in R^{3 \times 1}$  represents the actuator space that is related to the robot joint-space as [Chapters 6–29]

$$\begin{aligned} x_a &= h(\theta) \\ \dot{x}_a &= J(\theta)\dot{\theta} \end{aligned} \tag{3}$$

where  $h(\theta) \in R^{3 \times 1}$  denotes the forward kinematics of the actuator and  $J(\theta) = \frac{\partial h}{\partial \theta} \in R^{3 \times 3}$  represents the differentiable actuator Jacobian matrix as shown in Appendix B.

The torque vector is calculated as follows [30]:

$$\tau = J(\theta)F_a = J(\theta)(A_1P_1 - A_2P_2) \tag{4}$$

where  $A_{i(i=1,2)} = \text{diag}(A_{i1}, \dots, A_{i3}) \in R^{3 \times 3}$  are an area matrix of piston head part and an area matrix of rod part.  $P_{i(i=1,2)} = [P_{i1} \ \dots \ P_{i3}]^T$  are the pressure vector of two chambers of each actuator.

The hydraulic actuator pressure dynamics can be presented as follows [31]:

$$\dot{P}_1 = \beta V_1^{-1}(x_a) \left[ -A_1 \frac{\partial x_a}{\partial \theta} \dot{\theta} + \chi_1 [P_1, U[u]] U[u] \right] - \zeta_1(t) \tag{5}$$

$$\dot{P}_2 = \beta V_2^{-1}(x_a) \left[ A_2 \frac{\partial x_a}{\partial \theta} \dot{\theta} - \chi_2 [P_2, U[u]] U[u] \right] + \zeta_2(t) \tag{6}$$

where  $\beta$  is the effective bulk modulus,  $V_i(\theta)_{(i=1,2)} = \text{diag}(V_{i1}(\theta), \dots, V_{i3}(\theta)) \in R^{3 \times 3}$  are volume matrix of two chambers,  $V_{ij} = V_{ij0} + (-1)^{i+j} x_{ja} A_{ij}$ , ( $i = 1, 2; j = 1, 2, 3$ ),  $V_{ij0}$  ( $i = 1, 2; j = 1, 2, 3$ ) is initial volumes of two chambers,  $\zeta_i(t)_{(i=1,2)} \in R^{3 \times 1}$  are the lumped disturbances of two chambers (internal/external leakage, modelling error),  $U = [u_1 \ u_2 \ u_3]^T$  is a control voltage vector,  $\chi_i(P_i, U)_{(i=1,2)} = K_{qi} \text{diag}(\xi_{i1}, \dots, \xi_{i3}) \in R^{3 \times 3}$ , and  $K_{qi} = \text{diag}(k_{qi1}, \dots, k_{qi3}) \in R^{3 \times 3}$  are flow gain coefficients matrices in orifice equations of the actuators.

$$\begin{cases} \xi_{1i\{i=1,\dots,3\}} = \sqrt{P_s - P_{1i}}, u_i \geq 0 \\ \xi_{1i\{i=1,\dots,3\}} = \sqrt{P_{1i} - P_r}, u_i < 0 \\ \xi_{2i\{i=1,\dots,3\}} = \sqrt{P_{2i} - P_r}, u_i \geq 0 \\ \xi_{2i\{i=1,\dots,3\}} = \sqrt{P_s - P_{2i}}, u_i < 0 \end{cases} \tag{7}$$

where  $P_s$  and  $P_r$  are the supply pressure and the tank pressure, respectively.

### 2.3. State Space Form

Define the state variable vector:  $x_i (i = 1, 2, 3) \in R^{3 \times 1}$ ,  $x = [x_1, x_2, x_3]^T \triangleq [\theta, \dot{\theta}, [A_1P_1 - A_2P_2]]^T \in R^{9 \times 1}$ . Then, the state space system is derived as follows:

$$\begin{aligned} \dot{x}_1 &= x_2 \\ \dot{x}_2 &= M_0^{-1}(-C_0(x_1, x_2)x_2 - G_0(x_1) - \Delta U - d + \tau) \\ \dot{x}_3 &= -(\kappa_1(x_1)A_1 + \kappa_2(x_1)A_2) \frac{\partial x_a}{\partial x_1} x_2 + (\kappa_1(x_1)\xi_1(P_1, U) + \kappa_2(x_1)\xi_2(P_2, U))U + \Delta_2(t) \end{aligned} \tag{8}$$

where  $\kappa_i(x_1) = \beta A_i V_i^{-1}(x_1) \in R^{3 \times 3}$  ( $i = 1, 2$ ),  $\Delta_1(t) = \Delta U + d$ , and  $\Delta_2(t) = A_1 \zeta_1(t) - A_2 \zeta_2(t)$ .

The Equation (8) can be rewritten as follows

$$\begin{aligned} \dot{x}_1 &= x_2 \\ \dot{x}_2 &= M_0^{-1}(-C_0(x_1, x_2)x_2 - G_0(x_1) - \Delta_1(t) + J(x)x_3) \\ \dot{x}_3 &= F_1x_2 + F_2U + \Delta_2(t) \end{aligned} \tag{9}$$

where  $F_1 = -[\kappa_1A_1 + \kappa_2A_2]\frac{\partial x_a}{\partial x_1} \in R^{3 \times 3}$ , and  $F_2 = \kappa_1\zeta_1(P_1, U(u)) + \kappa_2\zeta_2(P_2, U(u)) \in R^{3 \times 3}$ .

**Remark 1.** In practice,  $\det(\zeta_1(P_1, U(u)))$  and  $\det(\zeta_2(P_2, U(u)))$  are both seldom zero when the system is operating smoothly, since  $P_1$  and  $P_2$  are rarely close to  $P_s$  and  $P_r$ . In the seldom case that  $\det(\zeta_1(P_1, U(u)))$  and  $\det(\zeta_2(P_2, U(u)))$  equal to zero (e.g., due to the noise in  $P_1$  and  $P_2$ ) it is set to a small positive number to avoid the problem of dividing zero.

### 3. Control Design

#### 3.1. Sliding Mode Control with a Backstepping Technique

In this research, a robust control via the backstepping approach [19] and sliding mode control [32] is designed to control the position of the manipulator. The proposed control is divided into two control loops to control the manipulator dynamic and regulate the hydraulic dynamic. One control is a conventional sliding model [33] which handles the manipulator dynamic to generate the desired torque for the hydraulic control. In the hydraulic dynamic, an ISMC is employed to control torques under the presence of the uncertainties and the nonlinear terms.

**Step 1:** The sliding mode control for the manipulator dynamics.

Definite state variable errors  $e = x_1 - x_{1d} \in R^{3 \times 1}$ ,  $\dot{e} = x_2 - x_{2d} \in R^{3 \times 1}$ , and  $\ddot{e} = \dot{x}_2 - \dot{x}_{2d} \in R^{3 \times 1}$ . The sliding variable vector  $s_1 = \begin{bmatrix} s_{11} & s_{12} & s_{13} \end{bmatrix}^T \in R^{3 \times 1}$  is chosen as follows:

$$s_1 = \dot{e} + \lambda_1 e \tag{10}$$

where  $\lambda_1 = \text{diag}(\lambda_{11}, \lambda_{12}, \lambda_{13})$  is a positive-definite matrix.

The reference state of the manipulator is defined as

$$\begin{cases} x_{2s} = x_2 - s_1 = x_{2d} - \lambda_1 e \in R^{3 \times 1} \\ \dot{x}_{2s} = \dot{x}_2 - \dot{s}_1 = \dot{x}_{2d} - \lambda_1 \dot{e} \in R^{3 \times 1} \end{cases} \tag{11}$$

The derivative of the sliding variable with respect to time is expressed as follows:

$$\dot{s}_1 = \ddot{e} + \lambda_1 \dot{e} \tag{12}$$

Replacing (10)–(12) into the 2nd equation of (9) yields:

$$M_0(q)\dot{s}_1 = J(x_1)x_3 - \Delta_1(t) - M_0(x_1)\dot{x}_{2s} - C_0(x_1, x_2)x_{2s} - G_0(x_1) - \frac{1}{2}\dot{M}_0(x_1)s_1 \tag{13}$$

The desired torques are chosen as follows:

$$x_{3d} = J(x_1)^{-1} \left( C_0(x_1, x_2)x_{2s} + G_0(x_1) + M_0(x_1)\dot{x}_{2s} - K_1s_1 - \eta \tanh\left(\frac{s_1}{\psi_1}\right) \right) \tag{14}$$

where  $K_1 = \text{diag}(k_{11}, \dots, k_{13}) \in R^{3 \times 3}$  is the positive definite matrix,  $\eta_1 = \text{diag}(\eta_{11}, \dots, \eta_{13}) \in R^{3 \times 3}$  is the positive definite matrix, it is chosen how to  $\eta_{1i} > |\Delta_{1i}|t$  ( $i = 1, \dots, 3$ ), and  $\psi_1 = \begin{bmatrix} \psi_{11} & \psi_{12} & \psi_{13} \end{bmatrix}^T \in R^{3 \times 1}$  is a width vector, and  $\tanh\left(\frac{s_1}{\psi_1}\right)$  is defined in Appendix C.

Definite the torque error vector

$$e_3 = x_3 - x_{3d} \tag{15}$$

with  $e_3 = [ e_{31} \ e_{32} \ e_{33} ]^T \in R^{3 \times 1}$ .

To prove to the stability and robustness of the manipulator, the Lyapunov candidate function is chosen as follows:

$$V_1(s_1) = \frac{1}{2} s_1^T M_0 s_1 \tag{16}$$

The derivative of the Lyapunov functions is presented as follows:

$$\dot{V}_1(s_1) = s_1^T M_0 \dot{s}_1 + \frac{1}{2} s_1^T \dot{M}_0 s_1 \tag{17}$$

Putting the Equations (14)–(16) into Equation (17) can yield to:

$$\dot{V}_1(s_1) = s_1^T e_3 - s_1^T K_1 s_1 + s_1^T \left( \Delta_1(t) - \eta_1 \tanh\left(\frac{s_1}{\psi_1}\right) \right) \tag{18}$$

The sliding variable,  $s_1$ , will converge to zero when the derivative of the Lyapunov function will be a negative semi-definite function. To ensure this condition, a robust control for the hydraulic dynamic is developed to guarantee that the torque error,  $s_2$ , will be bounded by  $\epsilon$ .

**Step 2:** Design the control, to assure the torque error is as small as possible. The integral sliding mode control is chosen as

$$s_2 = e_3 + \lambda_2 z_3 \tag{19}$$

where  $\lambda_2 = \text{diag}(\lambda_{21}, \lambda_{22}, \lambda_{23}) \in R^{3 \times 3}$  is an arbitrary positive matrix, and  $z_3 = \int_0^t e_3(t) dt \in R^{3 \times 1}$ .

The differential of the ISMC is

$$\begin{aligned} \dot{s}_2 &= \dot{x}_3 - \dot{x}_{3d} + \lambda_2 e_3 \\ &= F_1(x) + F_2(x)U(u) + \Delta_2(t) - \dot{x}_{3d} + \lambda_2 e_3 \end{aligned} \tag{20}$$

The control vector is chosen

$$u = F_2^{-1}(x) \left( \dot{x}_{3d} - F_1(x) - K_2 s_2 - \lambda_2 e_3 - s_1 - \eta_2 \tanh\left(\frac{s_2}{\psi_2}\right) \right) \tag{21}$$

where  $K_2 = \text{diag}(k_{21}, k_{22}, k_{23}) \in R^{3 \times 3}$  is an arbitrary positive matrix,  $\eta_2 = \text{diag}(\eta_{21}, \eta_{22}, \eta_{23}) \in R^{3 \times 3}$  is a robust gain positive diagonal matrix of the sliding mode control  $s_2$ , it is chosen how to  $\eta_{2i} > |\Delta_{2i}|t$  ( $i = 1, 2, 3$ ),  $\psi_2 = [ \psi_{21} \ \psi_{22} \ \psi_{23} ]^T \in R^{3 \times 1}$  is a width vector, and  $\tanh\left(\frac{s_2}{\psi_2}\right)$  is defined in Appendix C.

**Assumption 1.** The perturbation,  $\Delta_2(t)$ , varies with respect to time, and it is bounded  $\|\Delta_{2i}\|t\| \leq \eta_{2i}$  ( $i = 1, \dots, 3$ ).

Consider the Lyapunov function candidate

$$V_2(s_1, s_2) = V_1(s_1) + \frac{1}{2} s_2^T s_2 \tag{22}$$

The derivative of the Lyapunov function (22) is

$$\dot{V}_2(s_1, s_2) = \dot{V}_1(s_1) + s_2^T \dot{s}_2(t) \tag{23}$$

Replacing (21), and (18) into (23), the derivative of the Lyapunov function can be rewritten as follows:

$$\dot{V}_2(s_1, s_2) = \dot{V}_1(s_1) + s_2^T \dot{s}_2 = -\sum_{i=1}^2 \left( s_i^T K_i s_i + s_i^T (\Delta_i(t) - \eta_i \tanh(s_2)) \right) - z_3^T \lambda_2 s_1 \leq -\zeta^T \Xi \zeta + \delta \quad (24)$$

where  $\zeta = \begin{bmatrix} s_1 \\ z_3 \\ e_3 \end{bmatrix} \in R^{9 \times 1}$  and

$$\Xi = \begin{bmatrix} K_1 & -\frac{1}{2}\lambda_2 & 0 \\ -\frac{1}{2}\lambda_2 & \lambda_2^T K_2 \lambda_2 & K_2 \lambda_2 \\ 0 & \lambda_2^T K_2 & K_2 \end{bmatrix} \in R^{9 \times 9}.$$

To guarantee the stability and robustness of the controlled system, the  $\dot{V}_2(\zeta(t))$  is a negative-definite function. The parameters  $K_1$ ,  $K_2$ , and  $c_2$  are chosen how the matrix  $\Xi$  is a positive definite matrix.

### 3.2. Proposed Control

#### 3.2.1. Adaptive Approximation Based on RBFNN

As presented in Section 2, the uncertainties always exist in the system dynamics. They are smooth uncertainties and unsmooth uncertainties. This section presents two approximations via the Radial Basis Function Neural Network [18] to compensate the smooth uncertainties in the mechanical and hydraulic dynamics.

The RBFNN has three layers which are the input layer, hidden layer, and the output layer, which is employed to implement the approximations. The inputs and the output of the RBFNN are the tracking errors and the control input, respectively. The function of each layer is presented as follows:

The input layer rescaled the input variables,  $e_i (i = 1, \dots, m)$  to the next layers.

The hidden layer derives the input values with the Radius Basis function, Gaussian function, as follows:

$$\mu_{ijk} = \exp\left(\frac{-(E_i - m_{eijk})^T (E_i - m_{eijk})}{\sigma_{ijk}^2}\right) \quad (i=1,2;j=1,2,3;k=1,\dots,n) \quad (25)$$

where  $E_i = [e_{i1} \dots e_{im}]^T \in R^{m \times 1}$  is the input vector,  $m_{eijk} \in R^{m \times 1}$ , and  $\sigma_{ijk} (i = 1, 2; j = 1, 2, 3; k = 1, \dots, n) \in R^{m \times 1}$ , respectively, are the mean vector and the standard derivation of the Gaussian functions of the node  $ij$  in the hidden layer.

The output layer presents the compensation signals for the mechanical dynamic and the hydraulic dynamic as follows:

$$D_i = [d_{i1} \ d_{i2} \ d_{i3}]^T = W_i^T \mu_i \quad (26)$$

with  $W_i = \begin{bmatrix} \omega_{i11} & \dots & \omega_{i1n} & 0 & 0 & 0 & 0 \\ 0 & 0 & 0 & \dots & 0 & 0 & 0 \\ 0 & 0 & 0 & 0 & \omega_{i31} & \dots & \omega_{i3n} \end{bmatrix}^T \in R^{3n \times 3}, \mu_i =$

$\begin{bmatrix} \mu_{i11} & \dots & \mu_{i1n} & \mu_{i21} & \dots & \mu_{i2n} & \mu_{i31} & \dots & \mu_{i3n} \end{bmatrix}^T \in R^{3n \times 1}, (i = 1, 2)$  Each adaptive approximation includes RBFNNs and its adaptive laws and the online-tuning RBFNN is deployed to eliminate the smooth uncertainties in the mechanical dynamic and the hydraulic dynamic. These approximations reduce the chattering effects and improve the precisions. The adaptive laws

are derived from the Lyapunov approach. The approximations will compensate the mechanical uncertainties and the hydraulic uncertainties such that

$$D_i = D_i^* + \varepsilon_i = W_i^{*T} \mu_i(m_{ei}^*, \sigma_i^*) + \varepsilon_i, (i = 1, 2) \tag{27}$$

where  $\varepsilon_i = \begin{bmatrix} \varepsilon_{i1} & \varepsilon_{i2} & \varepsilon_{i3} \end{bmatrix}^T, (i = 1, 2)$  are reconstructed errors; and  $W_i^*, (i = 1, 2), m_{ei}^*, (i = 1, 2),$  and  $\sigma_i^*, (i = 1, 2)$  are optimal parameters of  $W_i, (i = 1, 2), m_{ei} = \begin{bmatrix} m_{ei11} & \cdots & m_{ei1n} & m_{ei21} & \cdots & m_{ei2n} & m_{ei31} & \cdots & m_{ei3n} \end{bmatrix}^T, (i = 1, 2) \in R^{3nm \times 1}$  and  $\sigma_i = \begin{bmatrix} \sigma_{i11} & \cdots & \sigma_{i1n} & \sigma_{i21} & \cdots & \sigma_{i2n} & \sigma_{i31} & \cdots & \sigma_{i3n} \end{bmatrix}^T \in R^{3nm \times 1}, (i = 1, 2)$  respectively, in the RBFNN. The approximation is expressed as the following form:

$$\hat{D}_i = \hat{W}_i^T \hat{\mu}_i(\hat{m}_{ei}, \hat{\sigma}_i), (i = 1, 2) \tag{28}$$

where  $\hat{W}_i, \hat{m}_{ei}, \hat{\sigma}_i$  are the estimated parameters of the RBFNN. An approximation error vector  $\tilde{D}_i$  is defined as follows:

$$\tilde{D}_i = D_i - \hat{D}_i = D_i^* + \varepsilon_i - \hat{D}_i = W_i^{*T} \mu_i^* - \hat{W}_i^T \mu_i + \varepsilon_i = \tilde{W}_i \mu_i^* + \hat{W}_i \tilde{\mu}_i + \varepsilon_i \tag{29}$$

where  $\tilde{W}_i = W_i^* - \hat{W}_i$  and  $\tilde{\mu}_i = \mu_i^* - \hat{\mu}_i$ . The RBFs are transformed into partially linear form by the Taylor series expansion, and the  $\tilde{\mu}$  can be represented as:

$$\tilde{\mu}_i = \begin{bmatrix} \tilde{\mu}_{i1} \\ \tilde{\mu}_{i2} \\ \vdots \\ \tilde{\mu}_{i[3n]} \end{bmatrix} = \mu_{mi} \tilde{m}_{ei} + \mu_{\sigma i} \tilde{\sigma}_i + v_i \tag{30}$$

where  $\tilde{m}_{ei} = m_{ei}^* - \hat{m}_{ei}; \tilde{\sigma}_i = \sigma_i^* - \hat{\sigma}_i; v \in R^{3n}$  is a vector of higher order terms;  $\mu_{mi} = \left[ \frac{\partial \mu_{i1}}{\partial m_{ei}} \quad \frac{\partial \mu_{i2}}{\partial m_{ei}} \quad \cdots \quad \frac{\partial \mu_{in}}{\partial m_{ei}} \right]^T \Big|_{m=\hat{m}} \in R^{3n \times 3nm};$  and  $\mu_{\sigma i} = \left[ \frac{\partial \mu_{i1}}{\partial \sigma_i} \quad \frac{\partial \mu_{i2}}{\partial \sigma_i} \quad \cdots \quad \frac{\partial \mu_{i[3n]}}{\partial \sigma_i} \right]^T \Big|_{\sigma_i=\hat{\sigma}_i} \in R^{3n \times 3nm}$ . The equation can be rewritten as follows:

$$\mu_i^* = \hat{\mu}_i + \mu_{mi} \tilde{m}_i + \mu_{\sigma i} \tilde{\sigma}_i + v_i \tag{31}$$

Replacing (31) into (29), it is presented that

$$\tilde{D}_i = \tilde{W}_i^T \hat{\mu}_i + \hat{W}_i^T \mu_{mi} \tilde{m}_i + \hat{W}_i^T \mu_{\sigma i} \tilde{\sigma}_i + \phi_i \tag{32}$$

where  $\phi_i = \tilde{W}_i^T \mu_{mi} \tilde{m}_i + \tilde{W}_i^T \mu_{\sigma i} \tilde{\sigma}_i + W_i^{*T} v_i + \varepsilon_i$

### 3.2.2. Adaptive Sliding Mode Control with a Backstepping Technique Based on RBFNN (ABSMC)

The virtual control (14) is represented as follows:

$$x_{3d} = J(x_1)^{-1} \left( C(x_1, x_2)x_{2s} + G(x_1) + M_0(x_1)\dot{x}_{2s} - K_1s_1 + \hat{D}_1 - \eta_1 \tanh\left(\frac{s_1}{\psi_1}\right) \right) \tag{33}$$

Additionally, the control input (21) is also rewritten as follows:

$$U = F_2^{-1}(x) \left( \dot{x}_{3d} - F_1(x) - K_2s_2 - \lambda_2e_3 - s_1 - \hat{D}_2 - \eta_2 \tanh\left(\frac{s_2}{\psi_2}\right) \right) \tag{34}$$

Then the Lyapunov function candidate is defined as

$$V_3 = V_2 + \frac{1}{2} \left( \sum_{i=1}^2 \text{trace} \left( \tilde{W}_i^T \Gamma_{1i}^{-1} \tilde{W}_i \right) + \tilde{m}_{ei}^T \Gamma_{2i}^{-1} \tilde{m}_{ei} + \sum_{i=1}^2 \tilde{\sigma}_i^T \Gamma_{3i}^{-1} \tilde{\sigma}_i \right) \tag{35}$$

where  $\Gamma_{ij} \in R^{3n \times 3n}$ ,  $(i = 1, \dots, 3, j = 1, 2)$  are positive definite matrices.

**Assumption 2.** The reconstructed errors,  $\phi_i = \tilde{W}_i^T \mu_m \tilde{m} + \tilde{W}_i^T \mu_\sigma \tilde{\sigma} + W_i^{*T} v + \varepsilon_i$ ,  $(i = 1, 2)$ , in the mechanical dynamics and hydraulic dynamics are bounded by  $\|\phi_i\|_1 < \hat{\eta}_i$ .

**Theorem 1.** The hydraulic manipulator is presented by (9), the indirect adaptive backstepping sliding mode control is designed by (33), (34), and the adaptive laws for the RBFNN parameters are chosen as (36)–(38) such that all the tracking error states ( $s_1$  and  $s_2$ ) converge to zero in a finite time. The stability and robustness of the proposed control and the adaptive laws are guaranteed via the Lyapunov theory.

$$\dot{\hat{W}}_i = \text{tr} \left( \Gamma_{1i} \left( (-1)^{i+1} \hat{\mu}_i s_i^T + \Lambda_{1i} W \hat{\cdot} \right) \right); (i = 1, 2) \tag{36}$$

$$\dot{\hat{m}}_{ei} = \Gamma_{2i} \left( (-1)^{i+1} \mu_{mi}^T \hat{W}_i s_i^T + \Lambda_{2i} \hat{m}_{ei} \right); (i = 1, 2) \tag{37}$$

$$\dot{\hat{\sigma}}_i = \Gamma_{3i} \left( (-1)^{i+1} \mu_{\sigma i}^T \hat{W}_i s_i^T + \Lambda_{3i} \hat{\sigma}_i \right); (i = 1, 2) \tag{38}$$

where  $\Gamma_{1j} \in R^{3n \times 3n}$ ,  $\Lambda_{1j} \in R^{3n \times 3n}$ ,  $(j = 1, 2)$ ,  $\Gamma_{ij} \in R^{3nm \times 3nm}$ ,  $\Lambda_{ij} \in R^{3nm \times 3nm}$ ,  $(i = 2, 3, j = 1, 2)$  are positive definite matrices, and

$$\text{tr} \left( \begin{bmatrix} a_{11} & \dots & a_{1n} & \dots & \dots & \dots & \dots & \dots & \dots \\ \dots & \dots & \dots & a_{21} & \dots & a_{2n} & \dots & \dots & \dots \\ \dots & \dots & \dots & \dots & \dots & \dots & a_{31} & \dots & a_{3n} \end{bmatrix}^T \right) = \begin{bmatrix} a_{11} & \dots & a_{1n} & 0 & 0 & 0 & 0 & 0 & 0 \\ 0 & 0 & 0 & a_{21} & \dots & a_{2n} & 0 & 0 & 0 \\ 0 & 0 & 0 & 0 & 0 & 0 & a_{31} & \dots & \omega_{3n} \end{bmatrix}^T$$

The differential Lyapunov function candidate (35) is expressed as follows:

$$\begin{aligned} \dot{V}_3 &= \dot{V}_2 - \sum_{i=1}^2 \text{trace} \left( \dot{\hat{W}}_i^T \Gamma_{1i}^{-1} \tilde{W}_i \right) - \sum_{i=1}^2 \tilde{m}_{ei}^T \Gamma_{2i}^{-1} \dot{\tilde{m}}_{ei} - \sum_{i=1}^2 \tilde{\sigma}_i^T \Gamma_{3i}^{-1} \dot{\tilde{\sigma}}_i \\ &= - \sum_{i=1}^2 \left( s_i^T K_i s_i + \left( \text{trace} \left( \hat{W}_i^T \Gamma_{1i}^{-1} \tilde{W}_i - (-1)^{i+1} s_i \mu_i^T \tilde{W}_i \right. \right. \right. \\ &\quad \left. \left. \left. + \left( \dot{\hat{m}}_{ei}^T \Gamma_{2i}^{-1} \tilde{m}_{ei} - (-1)^{i+1} s_i \hat{W}_i^T \mu_{im} \tilde{m}_{ei} \right) + \left( \dot{\hat{\sigma}}_i^T \Gamma_{3i}^{-1} \tilde{\sigma}_i - (-1)^{i+1} s_i \hat{W}_i^T \mu_{i\sigma} \tilde{\sigma}_i \right) + \phi_i - \eta_i \tanh \left( \frac{s_i}{\psi_i} \right) \right) s_i \right) \end{aligned} \tag{39}$$

Replacing (36), (37), and (38) into (39), we have

$$\dot{V}_3 = -\zeta^T \Xi \zeta - \sum_{i=1}^2 \left( \text{trace} \left( \tilde{W}_i^T \Lambda_{1i} \tilde{W}_i \right) + \tilde{m}_{ei}^T \Lambda_{2i} \tilde{m}_{ei} + \tilde{\sigma}_i^T \Lambda_{3i} \tilde{\sigma}_i + \left( \phi_i - \eta_i \tanh \left( \frac{s_i}{\psi_i} \right) \right) s_i \right) \tag{40}$$

Since  $-\tilde{(\cdot)}_i^T \Lambda_{ij} \tilde{(\cdot)}_i = -\tilde{(\cdot)}_i^T \Lambda_{ij} \left( (\cdot)_i^* + \tilde{(\cdot)}_i \right)$  and  $-\tilde{(\cdot)}_i^T \Lambda_{ij} (\cdot)_i^* \leq \frac{1}{2} \left( \tilde{(\cdot)}_i^T \Lambda_{ij} \tilde{(\cdot)}_i + (\cdot)_i^{*T} \Lambda_{ij} (\cdot)_i^* \right)$ , so we have  $-\tilde{(\cdot)}_i^T \Lambda_{ij} \tilde{(\cdot)}_i \leq -\frac{1}{2} \tilde{(\cdot)}_i^T \Lambda_{ij} \tilde{(\cdot)}_i + \frac{1}{2} (\cdot)_i^{*T} \Lambda_{ij} (\cdot)_i^*$ . Equation (40) can be represented as follows:

$$\begin{aligned} \dot{V}_3 &= -\zeta^T \Xi \zeta - \frac{1}{2} \sum_{i=1}^2 \left( \text{trace} \left( \tilde{W}_i^T \Lambda_i \tilde{W}_i + \tilde{m}_{ei}^T \Lambda_i \tilde{m}_{ei} + \tilde{\sigma}_i^T \Lambda_i \tilde{\sigma}_i \right. \right. \\ &\quad \left. \left. + \phi_i - \eta_i \text{stanh} \left( \frac{s_i}{\psi_i} \right) \right) s_i + \text{trace} W_i^{*T} \Lambda_i W_i^* \right) + m_{ei}^{*T} \Lambda_i m_{ei}^* + \sigma_i^{*T} \Lambda_i \sigma_i^* \leq -\kappa V_2 + C_\varepsilon \end{aligned} \tag{41}$$

where  $\kappa = \min(\lambda_{\min}(\Xi), \lambda_{\min}(M_1^{-1}K_1), \lambda_{\min}(K_2), \lambda_{\min}(\Gamma_{ij}\Lambda_{ij}))$ ,  $(i = 1, 2, 3, j = 1, 2)$  and  $C_\epsilon = \frac{1}{2}(\phi_i - \eta_i \text{sign}(s_i))s_i + m_{ei}^{*T} \Lambda_i m_{ei}^* + \frac{1}{2} \text{trace}(W_i^{*T} \Lambda_i W_i^*) + \frac{1}{2} \sigma_i^{*T} \Lambda_i \sigma_i^*$ .

From (41), and [34], we can conclude that the controlled system is ultimately uniformly bounded.

### 3.2.3. Switching Adaptive Laws

In this section, an adaptive law is developed on the robust gains to reject the unsmooth uncertainties. The adaptive laws are selected as follows:

$$\dot{\hat{\eta}}_i(t) = \begin{cases} \kappa_i \Gamma_{4i} \text{diag}\{|s_i|t\| & \text{if } \hat{\eta}_i\{t \geq 0 \text{ and } \|s_i\| > \epsilon_i \\ -\kappa_i \{\Gamma_{4i} \text{diag}\{|s_i|t\|}^{-1} & \text{if } \hat{\eta}_i\{t > 0 \text{ and } \\ & \epsilon_{i0} \leq \|s_i\| \leq \epsilon_i \\ 0 & \text{otherwise} \end{cases} \quad (42)$$

where  $\epsilon_i$  are threshold values of the adaptive laws,  $\kappa_i \in R^{3 \times 3}$  and  $\Gamma_{4i} \in R^{3 \times 3}$  are positive diagonal matrices,  $\tilde{\eta}_i = \eta_i - \hat{\eta}_i$ , and  $\hat{\eta}_i$  is estimated robust gains.

The adaptive robust gain laws (42) do not require knowledge of the upper boundary of the uncertainties. When the sliding variables stay out of a region that is smaller than  $\epsilon_i$ , the robust gains will quickly increase to force these variables to reach to the region. Otherwise, when the variables stay in the areas, the gains will decrease rapidly. These behaviors of the robust gain can reduce the chattering effects and ensure the robustness of the system.

**Proof.** The final Lyapunov function is modified as follow

$$V_0 = V_3 + \frac{1}{2} \sum_{i=1}^2 \gamma_i^{-1} \tilde{\eta}_i^T \Gamma_{4i}^{-1} \tilde{\eta}_i \quad (43)$$

The derivative of the Lyapunov function (43) is expressed as:

$$\dot{V}_0 = \dot{V} - \sum_{i=1}^2 \gamma_i^{-1} \tilde{\eta}_i^T \Gamma_{4i}^{-1} \dot{\hat{\eta}}_i \leq -\zeta^T \Xi \zeta - \sum_{i=1}^2 \left( \tilde{\eta}_i^T \left( |s_i| - \gamma_i^{-1} \Gamma_{4i}^{-1} \hat{\eta}_i \right) \right) \quad (44)$$

We consider two cases:  $\exists \|s_i\| \geq \epsilon_i$  and  $\forall \|s_i\| < \epsilon_i$ . When  $\exists \|s_i\| \geq \epsilon_i$ , applying (42) into (44), the derivative of a Lyapunov function is derived as follows:

$$\dot{V}_0 \leq -\zeta^T \Xi \zeta \quad (45)$$

It means that the Lyapunov function (43) is decreasing and bounded because  $0 \leq V_0(t) \leq V_0(0) \leq \infty$ .

When all sliding variables approach the small vicinity of the sliding manifold,  $\forall \|s_i\| \leq \epsilon_i$ , the derivative of a Lyapunov function is represented as:

$$\dot{V}_0 \leq -\zeta^T \Xi \zeta + \sum_{i=1}^2 \left( \tilde{\eta}_i^T \left( |s_i| + \Gamma_{4i}^{-1} \Gamma_{4i}^{-1} |s_i|^{-1} \right) \right) \quad (46)$$

The sliding variable  $s_i(t)$  will move away from the region  $|s_i| < \epsilon_i$  when the derivative Lyapunov function (14) becomes positive. Then, it will become negative again when the sliding variables leave the regions and the variables are driven back toward the regions. So, we can conclude that the controlled system is uniformly asymptotically stable [34].

## 4. Numerical Simulation and Experimental Studies

### 4.1. Numerical Simulations

We conducted some simulations in MATLAB2018a with sampling time of  $10^{-4}$  s and solver of ODE3. The manipulator dynamics is shown in Appendices A and B. The simulation structure is shown in Figure 2.

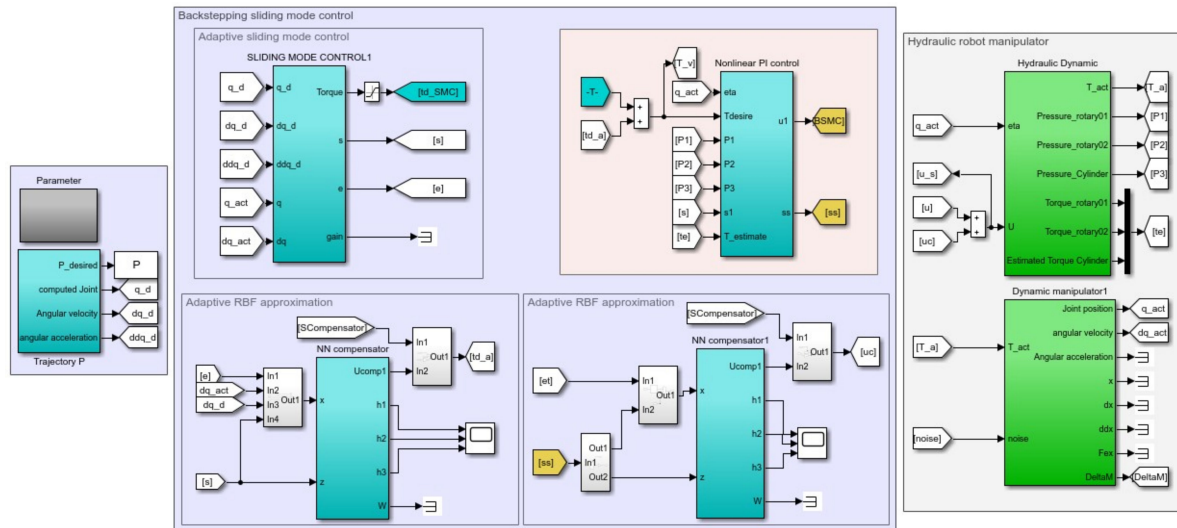


Figure 2. Simulation structure.

The parameters of the hydraulic manipulator are shown in Table 1.

Table 1. Parameters of the hydraulic manipulator.

Symbol	Value	Unit	Symbol	Value	Unit
$m_{i,i=1,\dots,3}$	5	kg	$A_{ij}(i,j=1,2)$	$15 \cdot 10^{-4}$	$m^2$
$l_1$	0.1	m	$A_{13}$	$15 \cdot 10^{-4}$	$m^2$
$l_2$	0.5	m	$A_{23}$	$10^{-3}$	$m^2$
$l_3$	0.2	m	$P_s$	100	bar
$g$	9.81	$m/s^2$	$P_r$	3	bar
$d_0$	0.2453	m	$k_{qij}(i,j=1,2)$	$2.16 \times 10^{-8}$	$m^3/\sqrt{Pa \cdot s \cdot V}$
$d_1$	0.2471	m	$k_{qi3}(i=1,2)$	$3.5 \times 10^{-8}$	$m^3/\sqrt{Pa \cdot s \cdot V}$
$d_2$	0.036	m	$\beta$	$1.25 \times 10^9$	$Nm^{-2}$

To verify the effectiveness of the proposed control, some simulations are implemented under the presence of the unknown variant payload, the unknown frictions and the unknown leakages in mechanical dynamics and hydraulic dynamics. They present not only the unmatched and matched uncertainties, but also the smooth and unsmooth uncertainties. Additionally, a backstepping sliding mode control (BSMC) and PI control are also carried out and their results are compared to the proposed control (ABSMC).

The unknown frictions are expressed as:

$$\tau_f = b_v \dot{\theta} + b_c \text{sign}(\dot{\theta}) \in R^{3 \times 1} \quad (47)$$

where  $b_v \in R^{3 \times 3}$  is a vicious positive matrix with  $b_v = \text{diag}([4, 4, 4]^T)$ , and  $b_c \in R^{3 \times 3}$  is a coulomb positive matrix with  $b_c = \text{diag}([4, 4, 4]^T)$ .

The leakages in hydraulic dynamics are derived by

$$Q_{LLi} = v_i(P_{i1} - P_{i2}), (i = 1, 2, 3) \tag{48}$$

where  $v_i$  is leakage coefficients with  $v = 1e^{-11}[20, 15, 1.5]^T$ .

The payload is alternated as shown in Figure 3.

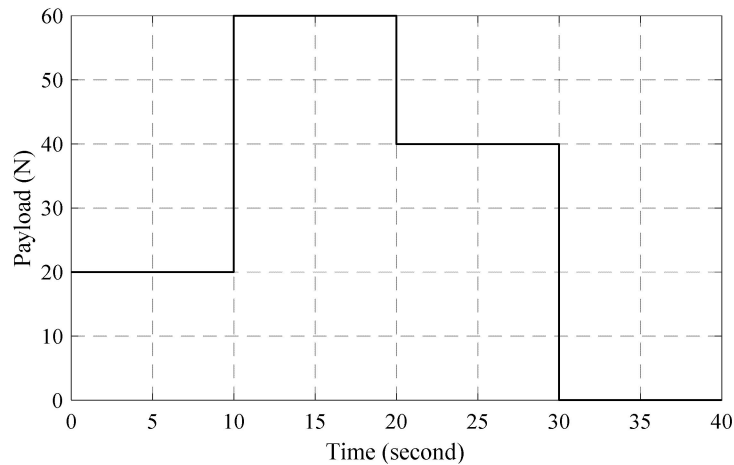


Figure 3. Payload performance.

The reference trajectories of the hydraulic manipulator are selected as  $x_d = [30 \sin[0.4\pi t, 20[1 + \sin[0.4\pi t + \pi/2, 50 + 30 \sin 0.4\pi t + \pi]]^T$ .

Each approximation in the position control has three inputs, 10 nodes in the hidden layer, and one output, and each approximation in the torque control has two inputs, 10 nodes in the hidden layer, and one output.

The parameters of the controllers are chosen by trial error method and shown in Table 2.

Table 2. Control Parameters.

Controller	Parameters
PID	$K_P = [60, 24, 15]^T, K_I = [32, 10, 8]^T, K_D = [0.4, 0.2, 0.1]^T$
BSMC	$c_1 = \text{diag}([60, 60, 40]), c_2 = \text{diag}([250, 1000, 50]), \eta_1 = 50\text{eye}(3), \eta_2 = 10^2\text{eye}(3), K_1 = \text{diag}([30, 25, 30]), K_2 = \text{diag}([10^3, 10^3, 5.10^4]);$
ABSMC	$\Gamma_{11} = 2\text{eye}(30), \Lambda_{11} = 2, 2.10^{-3}\text{eye}(30), \Gamma_{21} = 10.\text{eye}(90), \Lambda_{21} = 10^{-6}.\text{eye}(90), \Gamma_{31} = 10^{-6}\text{eye}(90), \Lambda_{31} = 10^{-5}\text{eye}(90), \varepsilon_1 = 10^{-4}[200, 1, 1]^T, \varepsilon_{10} = 10^{-2}\varepsilon_1 \Gamma_{41} = 6.10^3\text{eye}(3), \kappa_1 = \text{diag}([40, 40, 28]), \Gamma_{12} = 20e^{-4}\text{eye}(30), \Lambda_{12} = 4.4e^{-3}\text{eye}(30), \Gamma_{22} = 10\text{eye}(60), \Lambda_{22} = 10^{-6}\text{eye}(60), \Gamma_{32} = 10^{-6}\text{eye}(60), \Lambda_{32} = 10^{-5}\text{eye}(60), \varepsilon_2 = [1, 1, 1]^T, \varepsilon_{20} = 10^{-2}\varepsilon_2, \Gamma_{42} = 6.10^3\text{eye}(3), \kappa_2 = \text{diag}([0.2, 0.2, 0.14]).$

**Remark 2.** In order to show the ability of the proposed control, the parameters of control are designed with payload 20 N and keep with other payloads.

**Remark 3.** The proposed control is developed from the BSMC, so some parameters of SMCs in the proposed control are inherited from the BSMC.

Figures 4 and 5 plots the position responses and the position errors of the joints with three controllers, PID, BSMC, and ABSMC. The results showed that the nonlinearities, uncertainties and variant payloads impacted the accuracy of the controlled system with PID control. The nonlinearities which are caused by variant payloads are dealt by the BSMC. However, the remained errors are still significant. The proposed control with adaptive laws compensated the uncertainties and improved the accuracy of the controlled system, essentially.

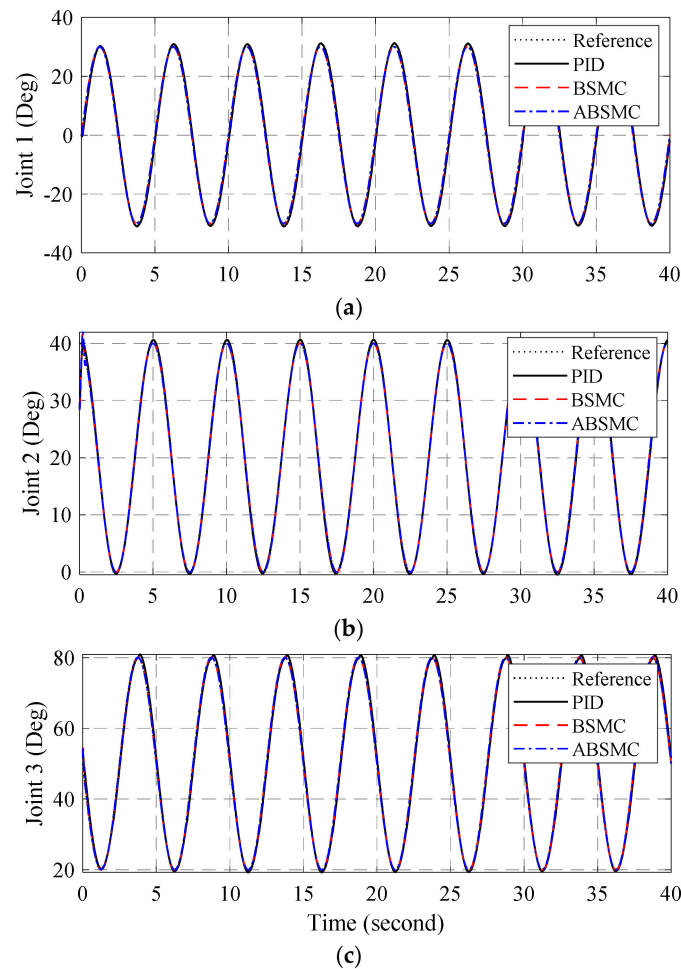


**Figure 4.** Joint responses of PID, BSMC, and ABSMC in (a) joint 1, (b) joint 2, (c) joint 3.

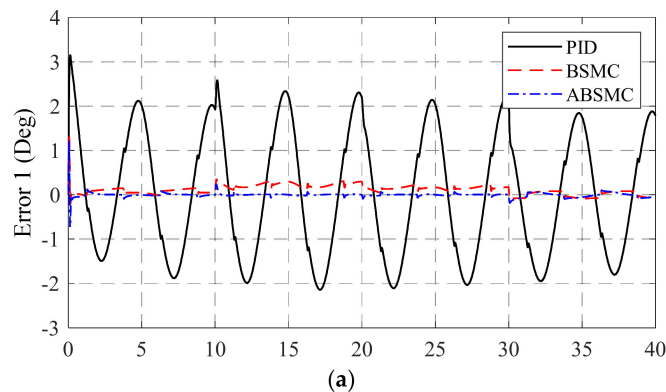


**Figure 5.** Cont.

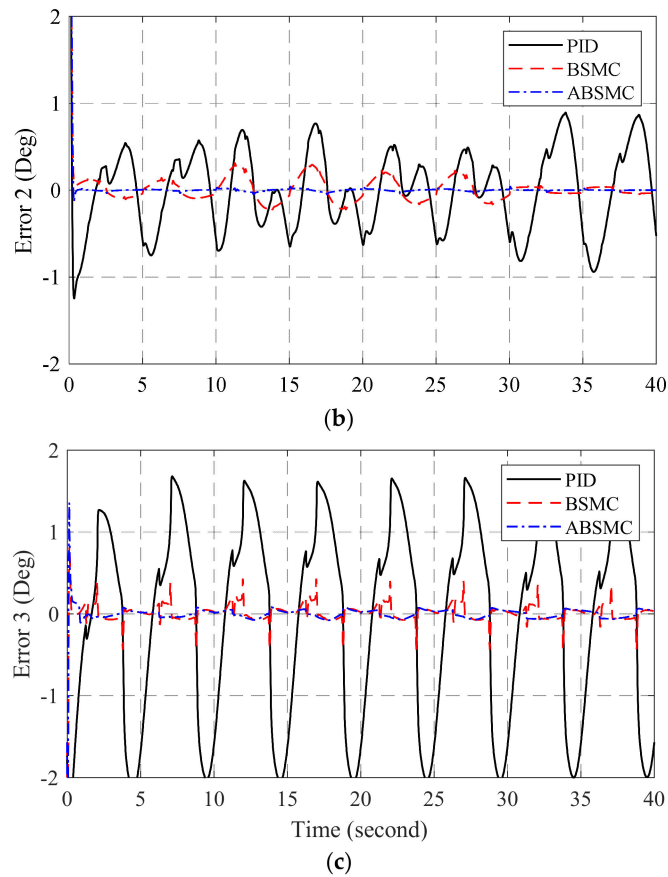


Figure 5. Joint errors of PID, BSMC, and ABSMC in (a) joint 1, (b) joint 2, (c) joint 3.

Figures 6 and 7 respectively show the torque performances and torque errors at each joint of the two controllers which are the BSMC and the proposed control. The virtual torques were calculated by (14) and (33) with the BSMC and the proposed control, respectively. The estimated torques were computed based on pressures from two chambers. The results proved that the proposed control with the adaptive mechanisms regulated the torque responses better than the BSMC. Figure 8 shows the control signals of the BSMC and the proposed controller.

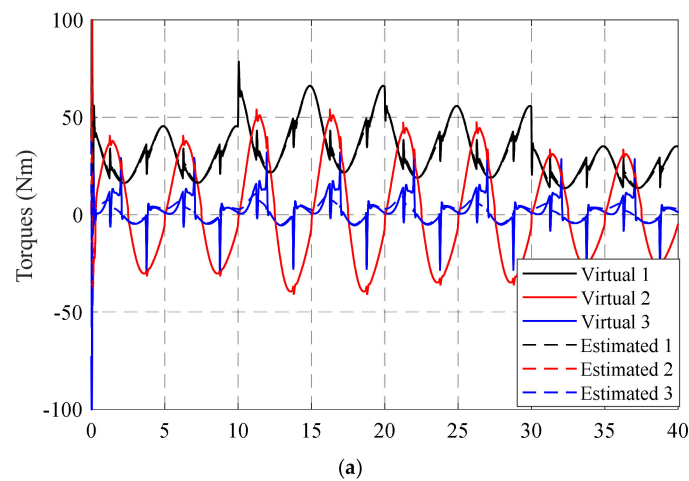


Figure 6. Cont.

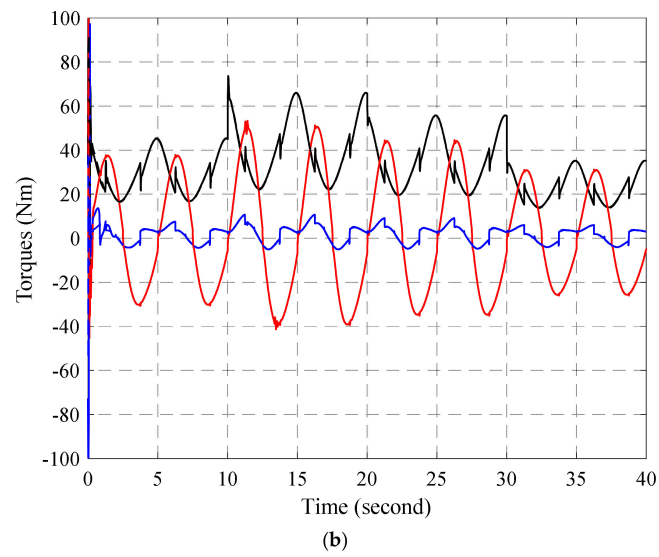


Figure 6. Torque responses with (a) BSMC, and (b) ABSMC.

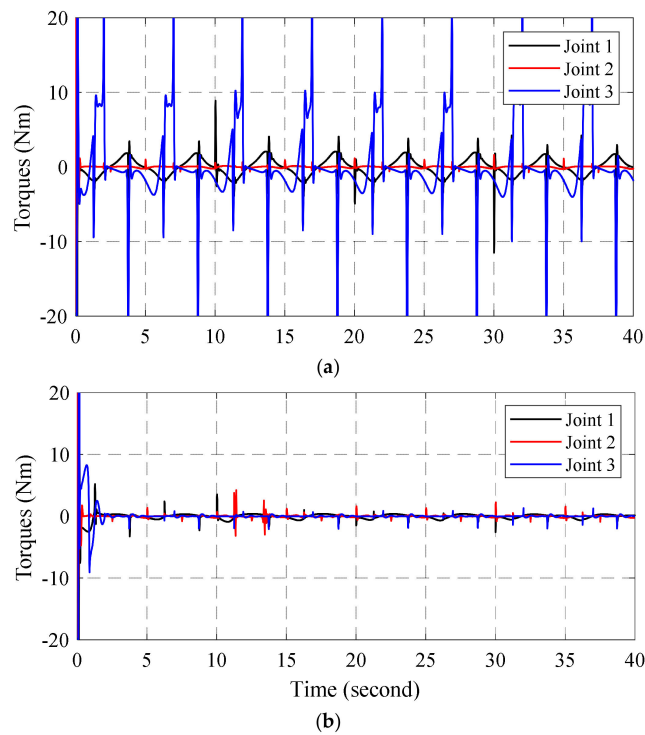


Figure 7. Torque errors with (a) BSMC, and (b) ABSMC.

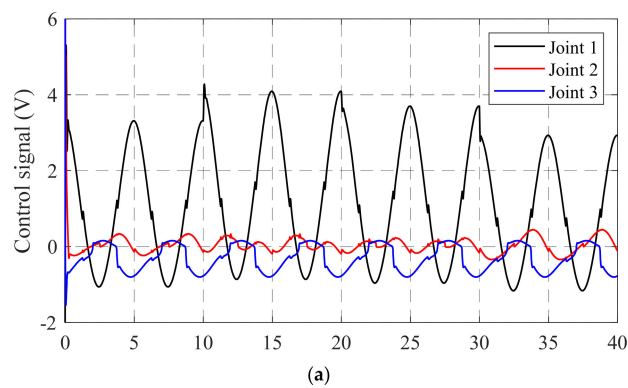


Figure 8. Cont.

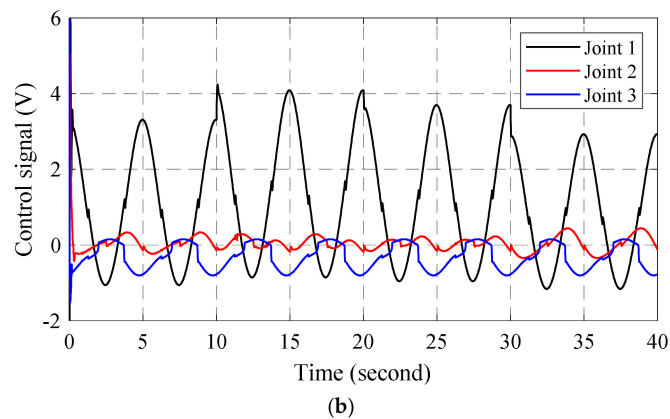


Figure 8. Control signals of (a) BSMC, and (b) ABSMC.

**Remark 4.** The simulation results proved that the proposed control compensated all uncertainties more effectiveness than the PID control and BSMC. The RBFNNs exhibited the approximately ability with the smooth uncertainties and the adaptive switching gains also demonstrate their ability for compensating the unsmooth uncertainties. However, the learning rates of adaptive laws have not mentioned in this paper. They will be intensively study in future work.

#### 4.2. Experimental Results

Furthermore, the proposed controller and backstepping controller are practically conducted on the hydraulic manipulator with load and without load of 20 N. The test bench includes a hydraulic power, a computer and a 3-DOF manipulator as shown in Figure 9. The hydraulic flow rates which are supplied to the actuator from the hydraulic power unit are driven by the servo valves. The computer is equipped PCI cards such as PCIE 6363, and Quad04 to provide the control signal to the servo valves and read the pressure sensors and encoder sensors at each joint. The control algorithms are practically carried out in MATLAB Simulink with the Real-time Windows target toolbox at sampling time of 10 ms.

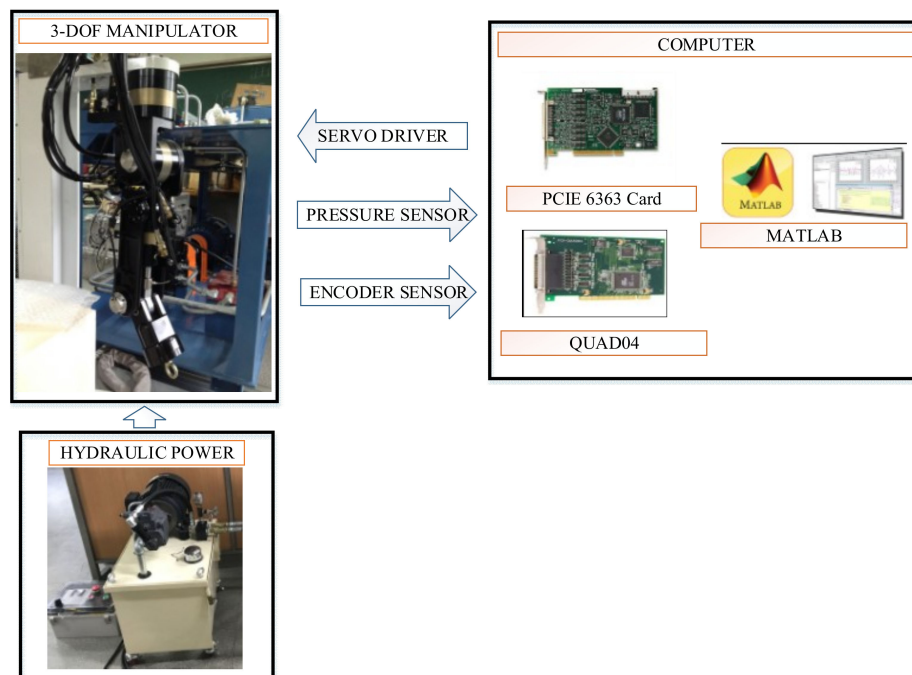


Figure 9. Structure of the test bench.

The control parameters are set to be backstepping sliding mode control:  $c_1 = \text{diag}([60, 70, 35])$ ,  $c_2 = \text{diag}([250, 850, 45])$ ,  $\eta_1 = 5\text{eye}(3)$ ,  $\eta_2 = 10^2\text{eye}(3)$ ,  $K_1 = \text{diag}([30, 25, 30])$ ,  $K_2 = \text{diag}([10^3, 10^3, 5.10^4])$ ; proposed control:  $\Gamma_{11} = 2\text{eye}(30)$ ,  $\Lambda_{11} = 2, 2.10^{-3}\text{eye}(30)$ ,  $\Gamma_{21} = 10.\text{eye}(90)$ ,  $\Lambda_{21} = 10^{-6}.\text{eye}(90)$ ,  $\Gamma_{31} = 10^{-6}\text{eye}(90)$ ,  $\Lambda_{31} = 10^{-5}\text{eye}(90)$ ,  $\varepsilon_1 = 10^{-4}[200, 1, 1]^T$ ,  $\varepsilon_{10} = 10^{-2}\varepsilon_1$ ,  $\Gamma_{41} = 5.10^3\text{eye}(3)$ ,  $\kappa_1 = \text{diag}([40, 40, 28])$ ,  $\Gamma_{12} = 20e^{-4}\text{eye}(30)$ ,  $\Lambda_{12} = 4.4e^{-3}\text{eye}(30)$ ,  $\Gamma_{22} = 10\text{eye}(60)$ ,  $\Lambda_{22} = 10^{-6}\text{eye}(60)$ ,  $\Gamma_{32} = 10^{-6}\text{eye}(60)$ ,  $\Lambda_{32} = 10^{-5}\text{eye}(60)$ ,  $\varepsilon_2 = [1, 1, 1]^T$ ,  $\varepsilon_{20} = 10^{-2}\varepsilon_2$ ,  $\Gamma_{42} = 5.10^3\text{eye}(3)$ ,  $\kappa_2 = \text{diag}([0.2, 0.2, 0.14])$ .

**Remark 5.** The initial weighting vectors of the RBFNNs are selected to be zero. Additionally, because the proposed control is developed based on the backstepping sliding mode control, some parameters of the proposed control are inherited from the backstepping sliding mode control.

**Remark 6.** The parameters of the controllers are adjusted when the manipulator operates without load. The parameters are kept in other case.

Figures 10–12 shows the joint responses, errors responses and control signals of the BSMC and proposed control when the hydraulic manipulator works without payload. In Figure 10, sinusoidal signals,  $x_{1d} = [30 \sin[0.628t], 20[1 + \cos[0.628t]], 20[2 - \sin[0.628t]]](\text{Deg.})$ , are set up as trajectories in the joints of the hydraulic manipulator and each subfigure presents for each joint response in the manipulator. The results show that the output responses of the BSMC and the proposed control track the reference signals. In Figure 11, the error performances of joints are provided in subfigures. The results demonstrate that the proposed control approximate the uncertainties to enhance accuracy of the control performance. The Figure 12 presents the control signals of the controllers.

Next experiments, the controllers are conducted on the hydraulic manipulator when the manipulator carry a payload of 20 N. The references are still sinusoidal signals as mentioned in previous case. Figures 13 and 14 present the error performances and control signals of the BSMC and the proposed control. The results in Figure 13 again prove that the adaptive approximators in the proposed control compensate not only the uncertainties such as unknown friction, modeling error and leakage but also the variant payload.

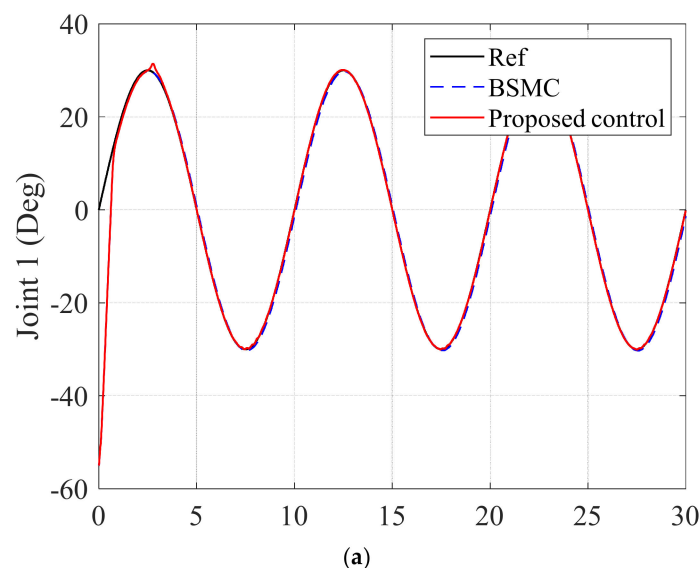


Figure 10. Cont.

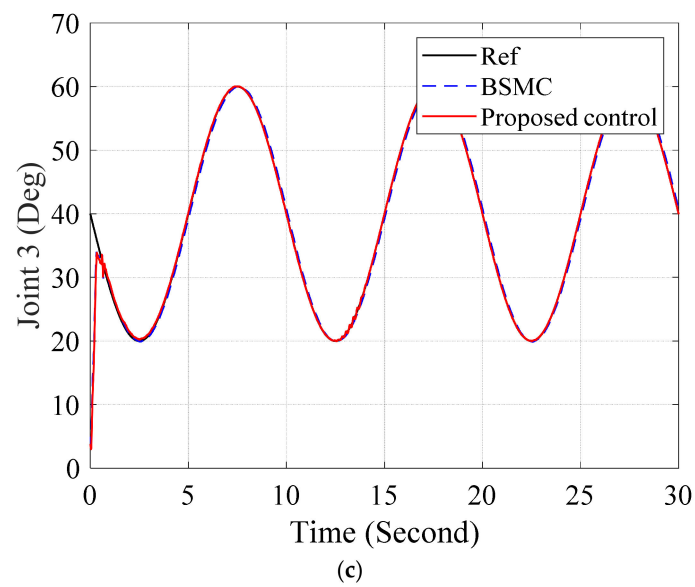
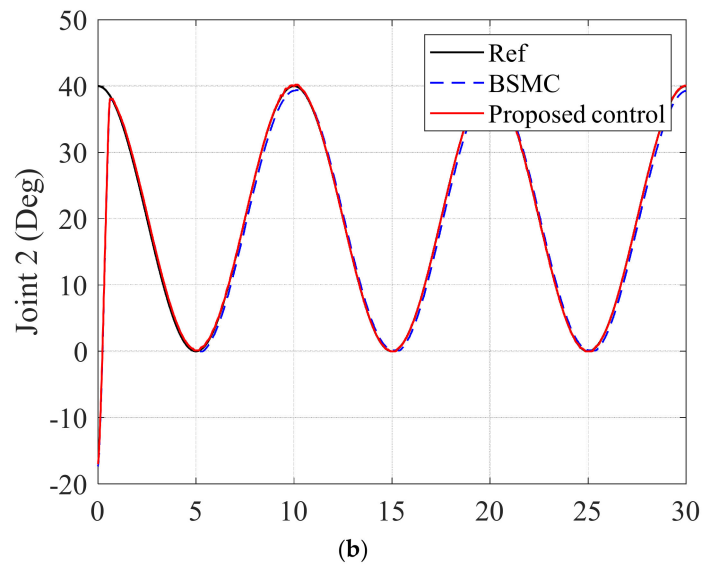


Figure 10. Joint responses of BSMC and proposed control in (a) joint 1, (b) joint 2, (c) joint 3 without load.

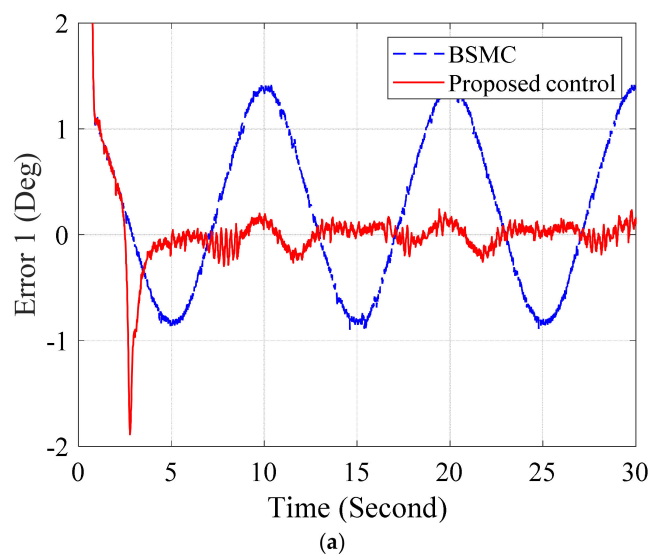
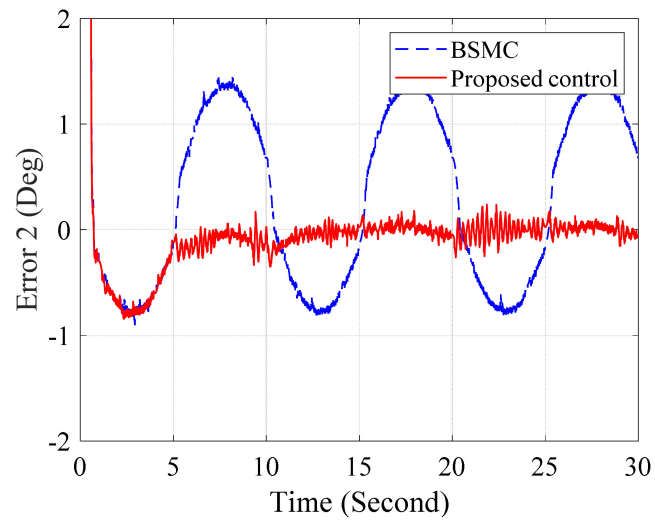
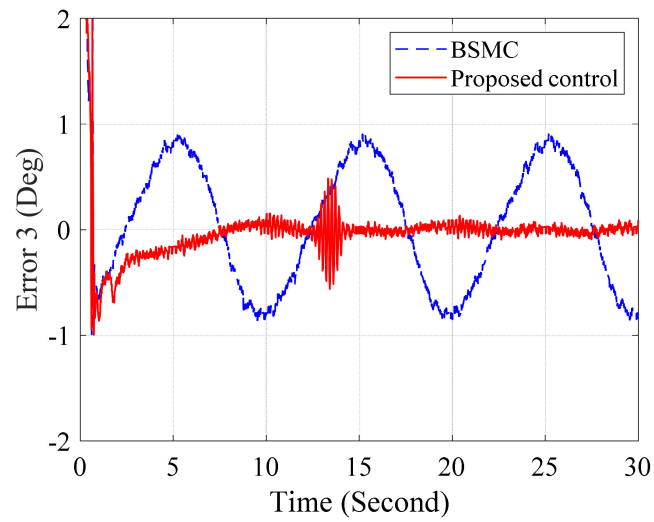


Figure 11. Cont.

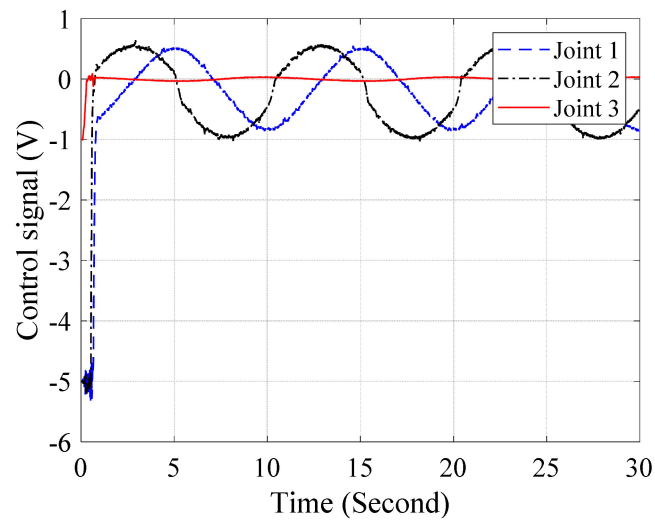


(b)



(c)

**Figure 11.** Error performance of BSMC and proposed control in (a) joint 1, (b) joint2, and (c) joint 3 without load.



(a)

**Figure 12.** Cont.

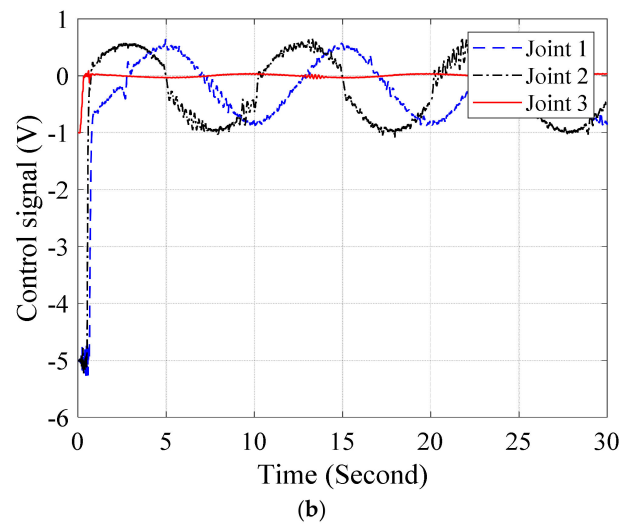


Figure 12. Control efforts of (a) BSMC and (b) Proposed control without load.

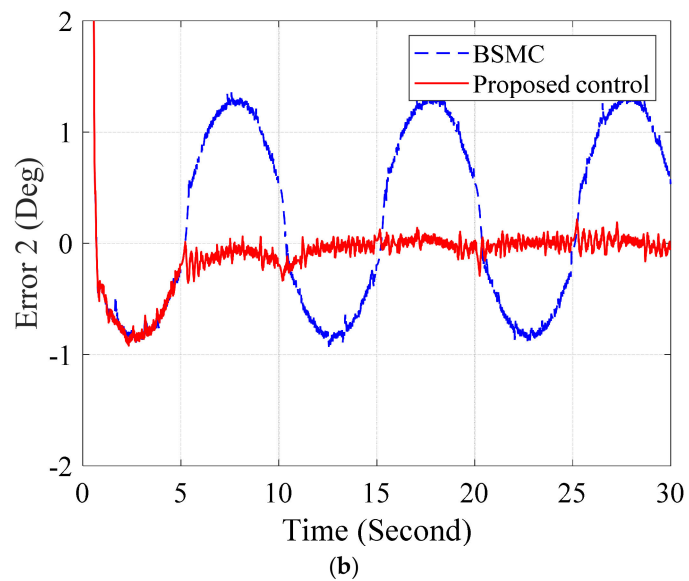
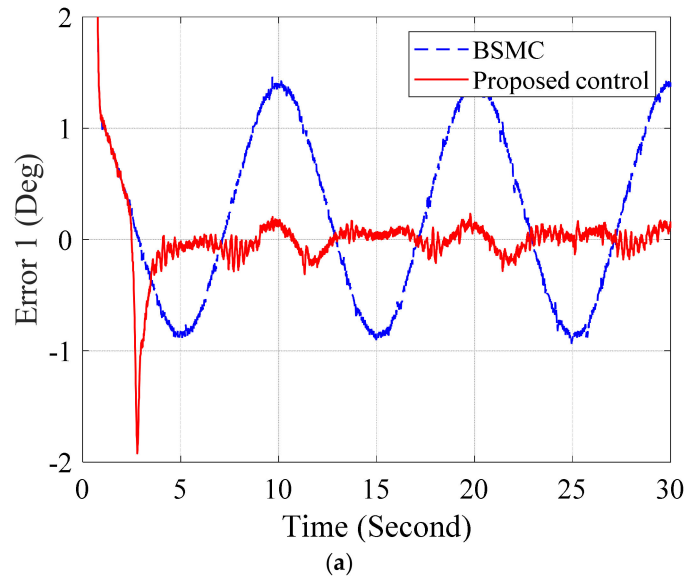
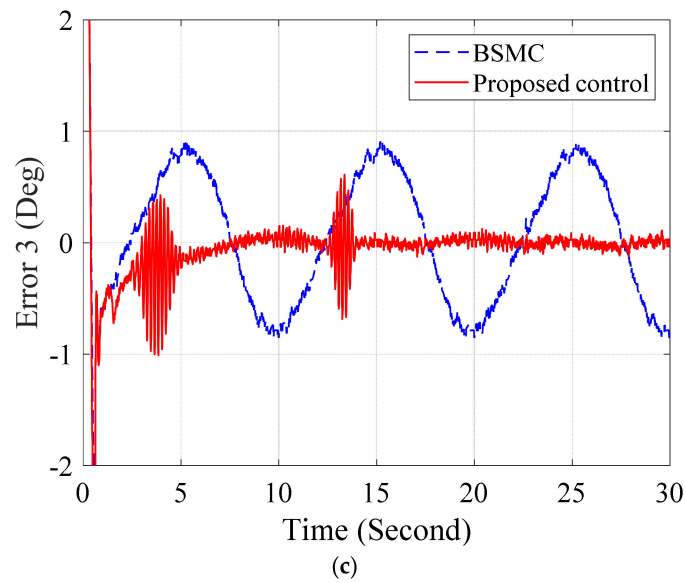
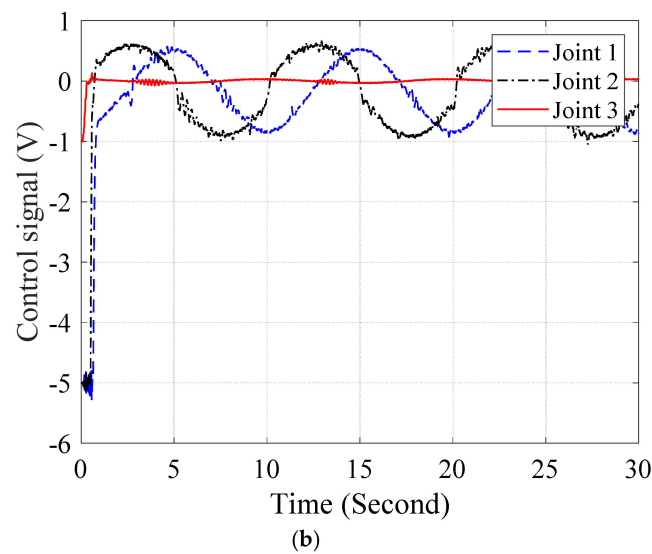
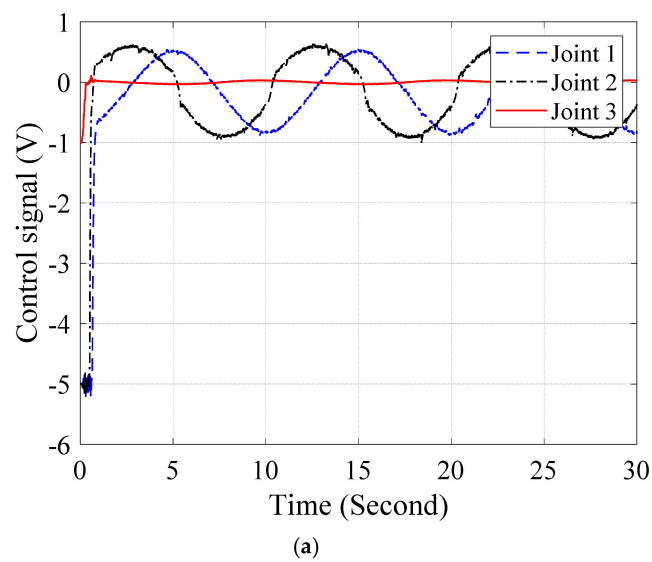


Figure 13. Cont.



**Figure 13.** Error responses of BSMC and proposed control in (a) joint 1, (b) joint 2, and (c) joint 3 with load.



**Figure 14.** Control efforts of (a) BSMC and (b) proposed control with load.

### 5. Conclusions

In this paper, an adaptive backstepping sliding mode control was proposed regarding tracking the position of the hydraulic manipulator including actuator dynamics under the presence of the unknown functions, the unknown variant payload, and leakages in mechanical and hydraulic dynamics. The uncertainties which present for the matched and unmatched uncertainties in the hydraulic manipulator are smooth and unsmooth functions. So, the proposition was developed based on backstepping sliding mode control, switching adaptive laws, and adaptive approximations. The adaptive approximators were developed based on RBFNN to deal with the smooth uncertainties. Specially, because the Taylor series expansion was used to analyze the RBFNN, so both the weighting vectors and parameters of the RBFs were tuning online to achieve the ideal parameters. The adaptive switching gains were provided to estimate the boundary of the unsmooth uncertainties without the predefined knowledge. The Lyapunov approach and backstepping technique were utilized together to prove the stability and robustness of the controlled system with the presence of all uncertainties. Finally, some simulations and experiments were implemented, and the results were compared to other controllers to demonstrate the effectiveness of the proposed control.

**Author Contributions:** K.K.A. was the supervisor providing funding and administrating the project, and he reviewed and edited the manuscript. D.-T.T. did the investigation, methodology, analysis and the validation, wrote the software, and wrote the original draft. H.-V.-A.T. checked the introduction and made the MATLAB software.

**Funding:** This work was supported by Basic Science Research Program through the National Research Foundation of Korea (NRF) funded by the Korean government (MEST) (NRF-2017R1A2B3004625).

**Conflicts of Interest:** The author declares no conflict of interest.

### Appendix A

According to Figures 1 and 2, the dynamic equations of a three-link robotic manipulator can be expressed as follows:

$$M_0(\theta)\ddot{\theta} + C_0(\theta, \dot{\theta})\dot{\theta} + G_0(\theta) + \Delta(t) = \tau \tag{A1}$$

$$\text{with } M_0(\theta) = \begin{pmatrix} m_{11} & 0 & 0 \\ 0 & m_{22} & m_{23} \\ 0 & m_{32} & m_{33} \end{pmatrix}, C_0(\theta, \dot{\theta}) = \begin{pmatrix} C_{11} & C_{12} & C_{13} \\ C_{21} & C_{22} & C_{23} \\ C_{31} & C_{32} & C_{33} \end{pmatrix}, \begin{matrix} m_{11} = m_3 l_3^2 s_{23}^2 + 2m_3 l_2 l_3 s_2 s_{23} + (m_2 + m_3) l_2^2 s_2^2 \\ m_{22} = (m_2 + m_3) l_2^2 + 2m_3 l_2 l_3 c_3 + m_3 l_3^2 \\ m_{23} = m_{32} = m_3 l_3^2 + m_3 l_2 l_3 c_3 \\ m_{33} = m_3 l_3^2 \end{matrix}$$

$$\begin{cases} C_{11} = m_3 l_3^2 c_{23} s_{23} (\dot{\theta}_2 + \dot{\theta}_3) + (m_2 + m_3) l_2^2 s_2 c_2 \dot{\theta}_2 \\ \quad + m_3 l_2 l_3 [s_2 c_{23} \dot{\theta}_2 + c_2 s_{23} (\dot{\theta}_2 + \dot{\theta}_3)] \\ C_{12} = m_3 l_3^2 s_{23} c_{23} \dot{\theta}_1 + m_3 l_2 l_3 s_2 c_2 \dot{\theta}_1 \\ \quad + (m_2 + m_3) l_2^2 s_2 c_2 \dot{\theta}_1 + m_3 l_2 l_3 c_2 s_{23} \dot{\theta}_1 \\ C_{13} = -c_{31} = m_3 l_3 \dot{q}_1 (2l_3 s_{23} c_{23} - l_2 s_3 + l_2 s_{23} c_2 + l_2 s_2 c_{23}) / 2 \\ C_{31} = -m_3 l_3 \dot{q}_1 (2l_3 s_{23} c_{23} - l_2 s_3 + l_2 s_{23} c_2 + l_2 s_2 c_{23}) / 2 \\ C_{32} = m_3 l_2 l_3 s_3 \dot{\theta}_2 \\ C_{33} = 0 \end{cases}, \begin{cases} C_{21} = -m_3 l_3^2 s_{23} c_{23} \dot{\theta}_1 - m_3 l_2 l_3 s_2 c_2 \dot{\theta}_1 \\ \quad - (m_2 + m_3) l_2^2 s_2 c_2 \dot{\theta}_1 - m_3 l_2 l_3 c_2 s_{23} \dot{\theta}_1 \\ C_{22} = -m_3 l_2 l_3 s_3 \dot{\theta}_3 \\ C_{23} = -m_3 l_2 l_3 s_3 (\dot{\theta}_2 + \dot{\theta}_3) \end{cases}$$

$$, G_0(\theta) = \begin{pmatrix} 0 \\ -m_3 l_3 g s_{23} - (m_2 + m_3) g l_2 s_2 \\ -m_3 l_3 g s_{23} \end{pmatrix},$$

$\theta = [\theta_1, \theta_2, \theta_3]^T, \dot{\theta} = [\dot{\theta}_1, \dot{\theta}_2, \dot{\theta}_3]^T, \ddot{\theta} = [\ddot{\theta}_1, \ddot{\theta}_2, \ddot{\theta}_3]^T, \tau = [\tau_1, \tau_2, \tau_3]^T, m_i$  are the weights of the  $i^{th}$  link ( $i = 1, 2, 3$ ) with  $s_{(\cdot)} = \sin((\cdot)), c_{(\cdot)} = \cos((\cdot)), s_{ij} = s_i c_j + c_i s_j, c_{ij} = c_i c_j - s_i s_j$ .

### Appendix B

The relationship among the rotational motion of the joint in joint space and of its actuator space with the motion of the end-effector in Cartesian space is examined. According to Figure A1, the rotational motion is driven by the movement of the cylinder can be expressed by:

$$d_3 = -\sqrt{d_1^2 + d_2^2 - 2d_1 \cdot d_2 \cos(\pi - \theta_3)} - d_0 \tag{A2}$$

where  $d_0$  is an initial length in case of maximum retracting,  $d_3$  is the length variable when the cylinder moves,  $d_1$  and  $d_2$  are fixed length of the hinge joints. Then taking derivative of the Equation (A2), we can obtain the correlational velocity between the joint motion and the cylinder motion:

$$\dot{d}_3 = \frac{\partial d_3}{\partial \theta_3} \dot{\theta}_3 = \frac{d_1 d_2 \sin(\pi - \theta_3)}{\sqrt{d_1^2 + d_2^2 - 2d_1 d_2 \cos(\pi - \theta_3)}} \dot{\theta}_3 = J_3(\theta_3) \dot{\theta}_3 \tag{A3}$$

with  $J_3(\theta_3)$  is the Jacobian vector of the 3rd joint.

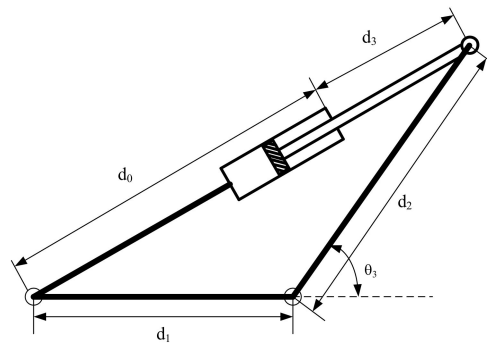


Figure A1. The mechanical structure between the cylinder and the joint 3rd.

Then the torque acting on the 3rd joint can be deduced by:

$$\tau_3 = J_3^T(\theta_3) F_3 \tag{A4}$$

The relationship between the actuator space and the joint space is shown as the below equations:

$$\begin{bmatrix} \theta_{1a} \\ \theta_{2a} \\ d_3 \end{bmatrix} = \begin{cases} \theta_1 \\ \theta_2 \\ -\left\{ \sqrt{d_1^2 + d_2^2 - 2d_1 \cdot d_2 \cos\{\pi - \theta_3\}} - d_0 \right\} \end{cases} \tag{A5}$$

with  $\theta_{ia}$  are angle of the actuators in the  $i^{th}$  ( $i = 1,2$ ) joint.

The Jacobian matrix between the joint space and actuator space is depicted as follows:

$$J = \begin{bmatrix} 1 & 0 & 0 \\ 0 & 1 & 0 \\ 0 & 0 & \frac{d_1 \cdot d_2 \cdot \sin[\pi - \theta_3]}{\sqrt{d_1^2 + d_2^2 - 2 \cdot d_1 \cdot d_2 \cdot \cos[\pi - \theta_3]}} \end{bmatrix} \tag{A6}$$

### Appendix C

The tan hyperbole functions are defined as follows:

$$\tanh\left(\frac{s_i}{\psi_i}\right) = \left[ \tanh\left[\frac{s_{i1}}{\psi_{i1}}\right] \quad \tanh\left[\frac{s_{i2}}{\psi_{i2}}\right] \quad \tanh\left[\frac{s_{i3}}{\psi_{i3}}\right] \right]^T \tag{A7}$$

where  $\psi_{ij}$ , ( $i = 1,2; j = 1,2,3$ ) are width values.

### References

1. Kamezaki, M.; Iwata, H.; Shigeki, S. A practical approach to detecting external force applied to hydraulic cylinder for construction manipulator. In Proceedings of the SICE Annual Conference 2010, Taipei, Taiwan, 18–21 August 2010; pp. 1255–1256.
2. Chen, Q.; Lin, T.; Ren, H. A Novel Control Strategy for an Interior Permanent Magnet Synchronous Machine of a Hybrid Hydraulic Excavator. *IEEE Access* **2018**, *6*, 3685–3693. [CrossRef]

3. Altare, G.; Vacca, A.; Richter, C. A novel pump design for an efficient and compact Electro-Hydraulic Actuator. In Proceedings of the 2014 IEEE Aerospace Conference, Big Sky, MT, USA, 1–8 March 2014; pp. 1–12.
4. Dong, W.; Han, S.; Jiao, Z.; Wu, S.; Zhao, Y. Compound angle-synchronizing control strategy for dual electro-hydraulic motors in hydraulic flight motion simulator. In Proceedings of the 2014 IEEE Chinese Guidance, Navigation and Control Conference, Yantai, China, 8–10 August 2014; pp. 2219–2224.
5. Raibert, M.; Blankespoor, K.; Nelson, G.; Playter, R. BigDog, the Rough-Terrain Quadruped Robot. *IFAC Proc. Vol.* **2008**, *41*, 10822–10825. [[CrossRef](#)]
6. Kuindersma, S.; Deits, R.; Fallon, M.; Valenzuela, A.; Dai, H.; Permenter, F.; Koolen, T.; Marion, P.; Tedrake, R. Optimization-based locomotion planning, estimation, and control design for the atlas humanoid robot. *Auton. Robot.* **2016**, *40*, 429–455. [[CrossRef](#)]
7. Dollar, A.M.; Herr, H. Lower Extremity Exoskeletons and Active Orthoses: Challenges and State-of-the-Art. *IEEE Trans. Robot.* **2008**, *24*, 144–158. [[CrossRef](#)]
8. Lee, J.; Chang, P.H.; Jin, M. Adaptive Integral Sliding Mode Control With Time-Delay Estimation for Robot Manipulators. *IEEE Trans. Ind. Electron.* **2017**, *64*, 6796–6804. [[CrossRef](#)]
9. Van, M.; Mavrouniotis, M.; Ge, S.S. An Adaptive Backstepping Nonsingular Fast Terminal Sliding Mode Control for Robust Fault Tolerant Control of Robot Manipulators. *IEEE Trans. Syst. Man and Cybern. Syst.* **2018**. [[CrossRef](#)]
10. Wai, R.J.; Muthusamy, R. Fuzzy-Neural-Network Inherited Sliding-Mode Control for Robot Manipulator Including Actuator Dynamics. *IEEE Trans. Neural Netw. Learn. Syst.* **2013**, *24*, 274–287. [[CrossRef](#)] [[PubMed](#)]
11. Wai, R.J.; Chen, P.C. Robust Neural-Fuzzy-Network Control for Robot Manipulator Including Actuator Dynamics. *IEEE Trans. Ind. Electron.* **2006**, *53*, 1328–1349. [[CrossRef](#)]
12. Wai, R.J.; Yang, Z.W. Adaptive Fuzzy Neural Network Control Design via a T-S Fuzzy Model for a Robot Manipulator Including Actuator Dynamics. *IEEE Trans. Syst. Man and Cybern. Part B Cybern.* **2008**, *38*, 1326–1346. [[CrossRef](#)]
13. Wang, L.; Chai, T.; Zhai, L. Neural-Network-Based Terminal Sliding-Mode Control of Robotic Manipulators Including Actuator Dynamics. *IEEE Trans. Ind. Electron.* **2009**, *56*, 3296–3304. [[CrossRef](#)]
14. Jing, Y. Adaptive control of robotic manipulators including motor dynamics. *IEEE Trans. Robot. Autom.* **1995**, *11*, 612–617. [[CrossRef](#)]
15. Huang, X.; Gao, H.; Li, J.; Mao, R.; Wen, J. Adaptive back-stepping tracking control of robot manipulators considering actuator dynamic. In Proceedings of the 2016 IEEE International Conference on Advanced Intelligent Mechatronics (AIM), Banff, AB, Canada, 12–15 July 2016; pp. 941–946.
16. Dinh, T.X.; Thien, T.D.; Anh, T.H.V.; Ahn, K.K. Disturbance Observer Based Finite Time Trajectory Tracking Control for a 3 DOF Hydraulic Manipulator Including Actuator Dynamics. *IEEE Access* **2018**, *6*, 36798–36809. [[CrossRef](#)]
17. Huang, A. A new adaptive controller for robot manipulators considering actuator dynamics. In Proceedings of the 2018 13th IEEE Conference on Industrial Electronics and Applications (ICIEA), Wuhan, China, 31 May–2 June 2018; pp. 476–480.
18. Wai, R.J.; Muthusamy, R. Design of Fuzzy-Neural-Network-Inherited Backstepping Control for Robot Manipulator Including Actuator Dynamics. *IEEE Trans. Fuzzy Syst.* **2014**, *22*, 709–722. [[CrossRef](#)]
19. Krstic, M.; Kanellakopoulos, I.; Kokotovic, P.V. *Nonlinear and Adaptive Control Design*; Wiley: Hoboken, NJ, USA, 1995.
20. Cong, B.; Liu, X.; Chen, Z. Backstepping based adaptive sliding mode control for spacecraft attitude maneuvers. *Aerosp. Sci. Technol.* **2013**, *30*, 1–7. [[CrossRef](#)]
21. Ahn, K.K.; Nam, D.N.C.; Jin, M. Adaptive Backstepping Control of an Electrohydraulic Actuator. *IEEE/ASME Trans. Mechatron.* **2014**, *19*, 987–995. [[CrossRef](#)]
22. Slotine, J.-J.E.; Li, W. *Applied Nonlinear Control*; Prentice Hall: Englewood Cliffs, NJ, USA, 1991; Volume 199.
23. Huang, Y.J.; Kuo, T.C.; Chang, S.H. Adaptive Sliding-Mode Control for Nonlinear Systems With Uncertain Parameters. *IEEE Trans. Syst. Man and Cybern. Part B Cybern.* **2008**, *38*, 534–539. [[CrossRef](#)]
24. Chu, Y.; Fei, J.; Hou, S. Dynamic global proportional integral derivative sliding mode control using radial basis function neural compensator for three-phase active power filter. *Trans. Inst. Meas. Control* **2017**. [[CrossRef](#)]

25. Fei, J.; Lu, C. Adaptive fractional order sliding mode controller with neural estimator. *J. Frankl. Inst.* **2018**, *355*, 2369–2391. [[CrossRef](#)]
26. Liu, S.; Zhou, H.; Luo, X.; Xiao, J. Adaptive sliding fault tolerant control for nonlinear uncertain active suspension systems. *J. Frankl. Inst.* **2016**, *353*, 180–199. [[CrossRef](#)]
27. Li, H.; Wang, J.; Du, H.; Karimi, H.R. Adaptive Sliding Mode Control for Takagi-Sugeno Fuzzy Systems and Its Applications. *IEEE Trans. Fuzzy Syst.* **2018**, *26*, 531–542. [[CrossRef](#)]
28. Zhang, Y.; Xu, Q. Adaptive Sliding Mode Control With Parameter Estimation and Kalman Filter for Precision Motion Control of a Piezo-Driven Microgripper. *IEEE Trans. Control Syst. Technol.* **2017**, *25*, 728–735. [[CrossRef](#)]
29. Murray, R.M.; Li, Z.; Sastry, S.S.; Sastry, S.S. *A Mathematical Introduction to Robotic Manipulation*; CRC Press: Boca Raton, FL, USA, 1994.
30. Yao, A.M.B. Indirect Adaptive Robust Control of Hydraulic Manipulators With Accurate Parameter Estimates. *IEEE Trans. Control Syst. Technol.* **2011**, *19*, 567–575. [[CrossRef](#)]
31. Manring, N. *Hydraulic Control Systems*; Wiley: Hoboken, NJ, USA, 2005.
32. Liu, J.; Wang, X. Adaptive Sliding Mode Control for Mechanical Systems. In *Advanced Sliding Mode Control for Mechanical Systems*; Springer: Berlin/Heidelberg, Germany, 2011; pp. 117–135.
33. He, J.; Luo, M.; Zhang, Q.; Zhao, J.; Xu, L. Adaptive Fuzzy Sliding Mode Controller with Nonlinear Observer for Redundant Manipulators Handling Varying External Force. *J. Bionic Eng.* **2016**, *13*, 600–611. [[CrossRef](#)]
34. Khalil, H.K. *Nonlinear Systems*; Prentice Hall: Upper Saddle River, NJ, USA, 2002.



© 2019 by the authors. Licensee MDPI, Basel, Switzerland. This article is an open access article distributed under the terms and conditions of the Creative Commons Attribution (CC BY) license (<http://creativecommons.org/licenses/by/4.0/>).